

Binary interactions and metallicity on the calibrations of star formation rate

Fenghui Zhang^{*1,2}, Lifang Li^{1,2}, Xiaoyu Kang^{1,2,3}, Yulong Zhuang^{1,2,3} and Zhanwen Han^{1,2}

¹National Astronomical Observatories/Yunnan Observatory, Chinese Academy of Sciences, Kunming, 650011, China

²Key Laboratory for the Structure and Evolution of Celestial Objects, Chinese Academy of Sciences, Kunming, 650011, China

³Graduate University of the Chinese Academy of Science, Beijing 100049, China

3 April 2019

ABSTRACT

Using the Yunnan evolutionary population synthesis (EPS) models with and without binary interactions, we present the luminosity of $H\alpha$ recombination line ($L_{H\alpha}$), the luminosity of $[OII]\lambda 3727$ forbidden-line doublet ($L_{[OII]}$), the ultraviolet (UV) fluxes at 1500 and 2800 Å ($L_{i,UV}$) and far-infrared flux (L_{FIR}) for burst, E, S0, Sa-Sd and Irr galaxies at $Z = 0.0001, 0.0003, 0.001, 0.004, 0.01, 0.02$ and 0.03 , present the conversion coefficients between star formation rate (SFR) and these diagnostics, and discuss the effects of binary interactions and metallicity on these SFR calibrations.

The inclusion of binary interactions can lower the SFR versus $L_{H\alpha}$ and SFR versus $L_{[OII]}$ conversion factors ($C_{H\alpha}$, $C_{[OII]}$) by ~ 0.1 - 0.2 dex, the SFR versus L_{1500} conversion factor (C_{1500}) by ~ 0.1 dex and the SFR versus L_{2800} conversion factor (C_{2800}) by ~ 0.2 - 0.1 dex, but raise the SFR versus L_{FIR} conversion factor (C_{FIR}) by ~ 0.05 dex. The differences in the $C_{H\alpha}$, $C_{[OII]}$ and C_{2800} caused by binary interactions are dependent of metallicity and those in the C_{1500} and C_{FIR} are independent of metallicity. The higher is the metallicity, the larger are the differences in the $C_{H\alpha}$ and $C_{[OII]}$, however, the smaller is the difference in the C_{2800} .

The ratio of the difference in the conversion factor caused by metallicity to the $[Fe/H]$ range, $\Delta C_{case,Z}/\Delta [Fe/H]$, reaches ~ 0.2 for $L_{H\alpha}$ and $L_{[OII]}$, ~ 0.1 for $L_{i,UV}$ and ~ 0.1 - 0.2 L_{FIR} . The $dC_{case,Z}/d[Fe/H]$ is different within different $[Fe/H]$ ranges and reaches the maximum value near the solar metallicity. At last, the $L_{i,UV}$ is not suitable to linear calibration of SFR at low metallicities.

We also obtain the $L_{H\alpha}$, $L_{[OII]}$, $L_{i,UV}$ and L_{FIR} for burst, E, S0, Sa-Sd and Irr galaxies by using the EPS models of BC03 ($0.0001 \leq Z \leq 0.05$), *SB99* ($0.0004 \leq Z \leq 0.05$), *PÉGASE* ($0.0001 \leq Z \leq 0.1$) and POPSTAR ($0.0001 \leq Z \leq 0.05$), present the conversion coefficients between SFR and these diagnostics, discuss the effects of the initial mass function and metallicity on these conversion coefficients, and compare the conclusions with those from our models.

Key words: binaries: general – galaxies: fundamental parameters – galaxies: general

1 INTRODUCTION

The luminosity of $H\alpha$ recombination line ($L_{H\alpha}$), the luminosity of $[OII]\lambda 3727$ forbidden line doublet ($L_{[OII]}$), the ultraviolet (UV, $L_{i,UV}$) and far-infrared (FIR, L_{FIR}) continuum fluxes are the commonly used traces of star formation rate (SFR, Kennicutt 1998). Gao & Solomon (2004) has even used HCN as an indicator of SFR. The calibrations of SFR in terms of these diagnostics are often obtained at solar metallicity and by using the evolutionary population synthesis (EPS) models without binary interactions, however, we

know that binary systems are common in the Universe and the stars are not always at solar metallicity.

Binary stars are common in the Universe. Upwards of 50% of field stars are in binary systems. In young massive stellar populations (SPs), the binary fraction is close to one (Kouwenhoven et al. 2007; Kobulnicky & Fryer 2007, also the references from Eldridge 2012). Moreover, in the Tarantula Nebula, the binary frequency among massive stars is high, with the ESO's VLT-FLAMES Tarantula Survey (VFTS) establishing that approximately two out of three massive stars are born in a binary system that will interact during their evolution (from Crowther 2012).

Zhang et al. (2004) have included binary interactions

* E-mail: gssephd@public.km.yn.cn; zhang-fh@hotmail.com

in the EPS models. Now, more and more studies began to pay an attention to the effect of binary interactions. Hernández & Bruzual (2011) have considered binary interactions in their EPS models. Sansom et al. (2009) have investigated the impact of binary-star yields on the spectra of galaxies. Zhang et al. (2009) have investigated the effect of binary interactions on the determination of photometric redshift for galaxies. Eldridge (2012) and Zhang et al. (2012) have investigated the effect of massive binaries and binaries on the SFR calibrations, respectively. Moreover, Hurley et al. (2005) have included binary interactions in the *Nbody4* code (Aarseth 1999). Spurzem (1999) and Anders et al. (2012) have included binaries in the *Nbody6++* and *STARLAB* codes, respectively. At last, some researchers have investigated the effect of binary interactions on the observations (de Grijs et al. 2008).

In Paper I (Zhang et al. 2012), we have discussed the effect of binary interactions on the SFR calibrations in terms of $L_{H\alpha}$, $L_{[OII]}$, $L_{i,UV}$ and L_{FIR} at solar metallicity. In this paper we will present the calibrations of SFR at non-solar metallicities and discuss the effects of binary interactions and metallicity on the SFR calibrations.

The outline of the paper is as follows. In Section 2 we describe the used EPS models and algorithms. In Section 3 we present the conversion coefficients between SFR and these tracers and discuss the effects of binary interactions and metallicity on these SFR calibrations. In Section 4 we present the conversion coefficients between SFR and these tracers by using the other EPS models and compare our results with those from them. Finally we present a summary and conclusions in Section 5.

2 MODELS AND ALGORITHMS

In order to present the SFR calibrations in terms of $L_{H\alpha}$, L_{1500} , L_{2800} , $L_{[OII]}$ and L_{FIR} , we need to present these parameters for various types of galaxies. First, it is to build various types of galaxies by advantage of EPS models and SFR, then it is to compute the above mentioned parameters for various types of galaxies. About the descriptions of various EPS models [including the Yunnan, BC03 (Bruzual & Charlot 2003), *STARBURST99* (hereafter *SB99*, Leitherer et al. 1999, 2010; Vázquez & Leitherer 2005), *PÉGASE* (Fioc & Rocca-Volmerange 1997, 1999) and POPSTAR (Mollá et al. 2009)], SFR, the method of building various types of galaxies and the algorithms of obtaining the above mentioned parameters, we have given in Paper I. Here, we only present the simple descriptions of EPS models, initial mass functions (IMF) and SFR. In Table 1, we present the name of each EPS model in the second column, the corresponding IMF [$\phi(M) = dN/dM$], the lower and upper mass limits (M_l and M_u) and metallicity Z in the third, fourth and fifth columns, respectively.

2.1 EPS models

As said above, the detailed description of various EPS models has been presented in Paper I, we refer the interested reader to part 2 for them. In Paper I we only use solar-metallicity EPS models and present the SFR calibrations at solar metallicity. In this paper, we use the EPS models at

several metallicities (see the fifth column of Table 1), i.e. in the second column of Table 1 in Paper I, the solar metallicity is replaced by several metallicities.

Moreover, for the *PÉGASE* EPS models, we do not use the default (i.e. consistent) evolution process of stellar metallicity, but present the results at individual metallicities.

2.2 IMF

• In the Yunnan models, the IMF of Miller & Scalo (1979, hereafter MS79) is used, its form is as follows:

$$\phi(M)_{MS79} \propto \begin{cases} M^{-1.4}, & 0.10 \leq M \leq 1.00, \\ M^{-2.5}, & 1.00 \leq M \leq 10.0, \\ M^{-3.3}, & 10.0 \leq M \leq 100., \end{cases} \quad (1)$$

where M is the stellar mass in units of M_\odot .

• In the BC03, *SB99*, *PÉGASE* and POPSTAR models, the Salpeter (1955, hereafter S55) IMF is used and its form is as follows: $\phi(M)_{S55} = M^{-\alpha}$, $\alpha = 2.35$ and the lower and upper mass limits are 0.1 (except the POPSTAR models) and 100. M_\odot . In the POPSTAR models, the lower mass limit of the S55 IMF is 0.15 M_\odot , which is different from that of the other EPS models, we call S55' IMF in Table 1.

• In the BC03 models, the used Chabrier (2003, hereafter Cha03) IMF is as follows:

$$\phi(M)_{Cha03} = \begin{cases} C_1 M^{-1} \exp\left[-\frac{(\log M - \log M_c)^2}{2\sigma^2}\right], & M \leq 1.0, \\ C_2 M^{-2.3}, & M > 1.0, \end{cases} \quad (2)$$

where $M_c = 0.08 M_\odot$, $\sigma = 0.69$ and M is the stellar mass in units of M_\odot . The lower and upper mass limits are 0.1 and 100. M_\odot .

• The IMF of Kroupa et al. (1993, hereafter K93), which is used in the *SB99* and *PÉGASE* models, is as follows:

$$\phi(M)_{K93} = \begin{cases} C_1 M^{-1.3}, & 0.10 \leq M \leq 0.50, \\ C_2 M^{-2.3}, & 0.50 \leq M \leq 1.00, \\ C_3 M^{-2.7}, & 1.00 \leq M \leq 100., \end{cases} \quad (3)$$

where $C_1 = 0.035$, $C_2 = 0.019$, $C_3 = 0.019$ and M is the stellar mass in units of M_\odot . Because all coefficients in equation (3) are set to 1 for the *SB99* models in this study and also are 1 in the *PÉGASE* models, we call K93' IMF in Table 1.

• The IMF of Kroupa et al. (2001, hereafter K01), which is used in the POPSTAR models, is as follows:

$$\phi(M)_{K01} = \begin{cases} C_1 M^{-0.30}, & 0.01 \leq M \leq 0.08, \\ C_2 M^{-1.30}, & 0.08 \leq M \leq 0.50, \\ C_3 M^{-2.30}, & 0.50 \leq M \leq 100., \end{cases} \quad (4)$$

where M is the stellar mass in units of M_\odot . In the POPSTAR models, $M_l = 0.15 M_\odot$.

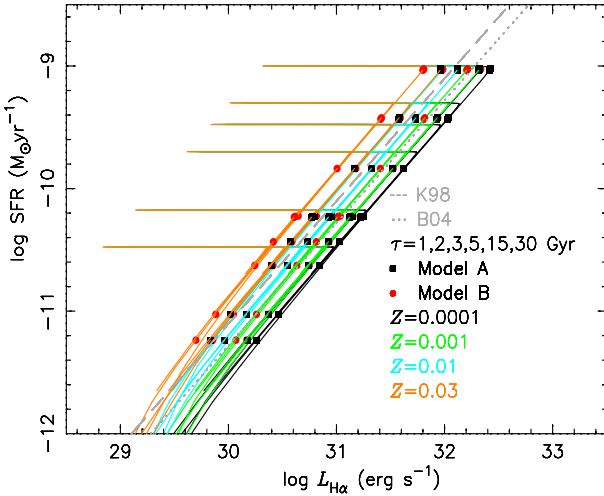
2.3 SFR

Various SFR forms are used to transform SP to galaxies. We use a δ -form SFR, six exponentially decreasing SFRs with characteristic time decays $\tau = 1, 2, 3, 5, 15$ and 30 Gyr and a constant-form SFR to build burst, E, S0, Sa-Sd and Irr types of galaxies, respectively. The exponentially decreasing SFR is given by

$$\psi(t) = [1 + \epsilon M_{PG}(t)] \tau^{-1} \exp(-t/\tau), \quad (5)$$

Table 1. Definition of Models (the first column) and description of the used EPS models (from the second to the last columns, including the name of each EPS model, IMF, the upper and lower mass limits M_l and M_u and metallicity Z).

Model	EPS name	IMF	M_l, M_u (M_\odot)	Z
A/B	Yunnan	MS79	0.10, 100	0.0001/0.0003/0.001/0.004/0.01/0.02/0.03
C-S55/Cha03	BC03	S55/Cha03	0.10, 100	0.0001/0.0004/0.004/0.008/0.02/0.05/- -
D-S55/K93'	SB99	S55/K93'	0.10, 100	- - - /0.0004/0.004/0.008/0.02/0.05/- -
E-S55/K93'	PÉGASE	S55/K93'	0.10, 100	0.0001/0.0004/0.004/0.008/0.02/0.05/0.10
F-S55'/K01	POPSTAR	S55'/K01	0.15, 100	0.0001/0.0004/0.004/0.008/0.02/0.05/- -

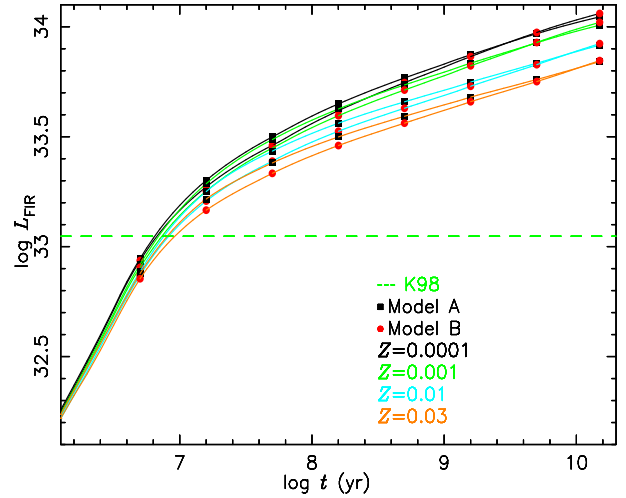
**Figure 1.** Relation between SFR and $L_{H\alpha}$ of E, S0, Sa, Sb, Sc and Sd galaxies [corresponding to $\tau = 1, 2, 3, 5, 15$ and 30 Gyr in equation (5), from top to bottom] for Models A (solid rectangles) and B (solid circles) at $Z = 0.0001$ (black), 0.001 (green), 0.01 (cyan) and 0.03 (red, from right to left). The ages of galaxies are in the range from 1 Myr to 15 Gyr. Also shown are the results of K98 (dashed line) and B04 (dotted line).

where τ is the e-folding time-scale, $M_{PG}(t) = [1 - \exp(-t/\tau)] - M_{stars} - M_{remnants}$ is the mass of gas that has been processed into stars and then returned to the ISM at t , M_{stars} and $M_{remnants}$ are the masses of stars and remnants at t , and ε denotes the fraction of $M_{PG}(t)$ that can be recycled into new star formation. In this work, $\varepsilon = 0$, i.e. the gas could not be recycled into new star formation.

3 EFFECTS OF BINARY INTERACTIONS AND METALLICITY ON SFR CALIBRATIONS

Using the Yunnan EPS models with and without binary interactions, various SFR and the algorithms described in Paper I, we obtain the luminosity of $H\alpha$ recombination line $L_{H\alpha}$, the luminosity of $[OII]\lambda 3727\text{\AA}$ forbidden line doublet $L_{[OII]}$, the UV fluxes at 1500 and 2800 \AA , $L_{i,UV}$, and FIR flux L_{FIR} of burst, E, S0, Sa-Sd and Irr galaxies at $Z = 0.0001, 0.0003, 0.001, 0.004, 0.01, 0.02$ and 0.03. For the sake of clarity, we refer to those using the Yunnan models with and without binary interactions as Models A and B, respectively.

Using these two sets of models, we will discuss the ef-

**Figure 3.** The L_{FIR} evolution of Irr galaxies (i.e. models with constant star formation, $SFR=1 M_\odot$) for Models A (solid rectangles) and B (solid circles) at $Z = 0.0001$ (black), 0.001 (green), 0.01 (cyan) and 0.03 (red, from top to bottom). Also shown is the result of K98 (green dashed line).

fects of binary interactions and metallicity on the SFR calibrations in terms of $L_{H\alpha}$, $L_{[OII]}$, $L_{i,UV}$ and L_{FIR} .

3.1 SFR versus $L_{H\alpha}$

In Fig. 1, we give the relation between $\log(SFR)$ and $\log(L_{H\alpha})$ (note the logarithmic scale) of E, S0, Sa-Sc and Sd galaxy types in the range from 0.1 Myr to 15 Gyr for Models A and B. For the sake of clarity, only the results at metallicity $Z=0.0001, 0.001, 0.01$ and 0.03 are presented. Also shown are the $SFR(L_{H\alpha})$ calibrations of K98 ($SFR_{H\alpha}/M_\odot \text{yr}^{-1} = 7.9 \times 10^{-42} L_{H\alpha}/\text{erg s}^{-1}$) and Brinchmann et al. (2004, hereafter B04, $SFR_{H\alpha}/M_\odot \text{yr}^{-1} = 5.25 \times 10^{-42} L_{H\alpha}/\text{erg s}^{-1}$). Both of calibration relations are linear and obtained at solar metallicity.

From Fig. 1, we see that the calibration curves of Models A and B at different metallicities are parallel to those of K98 and B04. That is to say, SFR varies linearly with $L_{H\alpha}$ at all Z . The calibration line moves upwards when increasing metallicity for both Models A and B. The reason is as follows. When increasing Z , the temperature of stars would decrease, hence the UV flux, the number of ionizing photons $Q(H)$ and $L_{H\alpha}$ [see equation (11) of Paper I] would decrease. Comparing the results between Models A and B at a given metallicity, we can obtain the effect of binary interactions

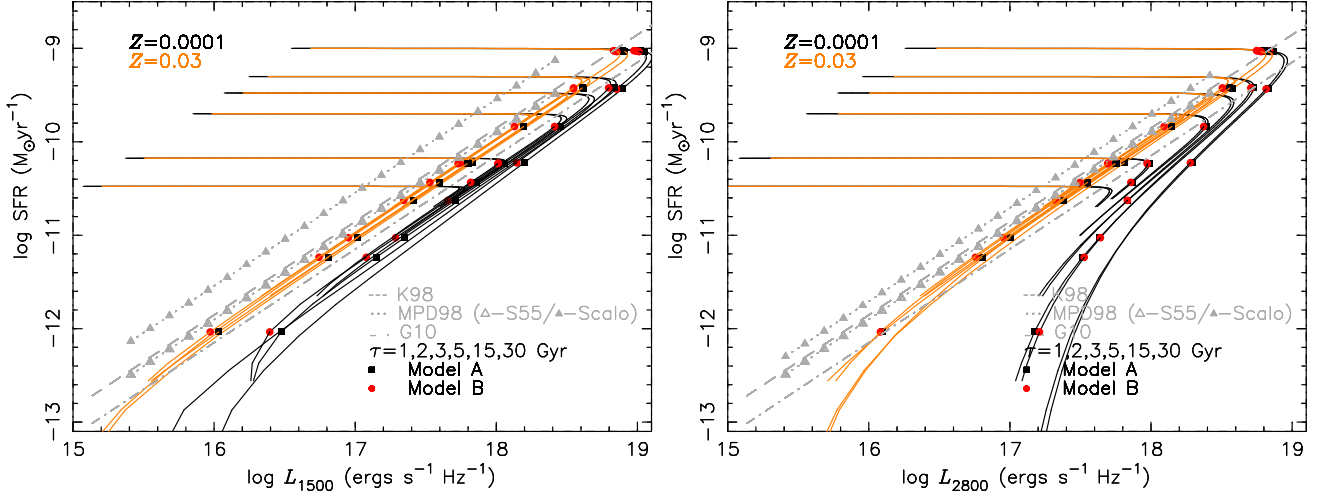


Figure 2. Relations between SFR and $L_{i,UV}$ of E, S0, Sa, Sb, Sc and Sd galaxies [corresponding to $\tau = 1, 2, 3, 5, 15$ and 30 Gyr in equation (5), from top to bottom] for Models A (solid rectangles) and B (solid circles) at $Z = 0.0001$ (black) and 0.03 (red, from right to left). Left-hand panel is for L_{1500} and right-hand panel is for L_{2800} . Also shown are the results of K98 (grey dashed line), MPD98 (grey dotted line, open and solid triangles are for using the S55 and Scalo IMFs, respectively) and G10 (grey dash-dotted line).

Table 2. Conversion coefficient between SFR and $L_{H\alpha}$ and the rms ($C_{H\alpha}$, $\sigma_{H\alpha}$) for Models A, B, C-S55/Cha03, D-S55/K93', E-S55/K93' and F-S55'/K01 at different metallicities. The top and bottom parts are for Models A-B and C-F, respectively. For each sub-part, the corresponding metallicities are given in the first line.

Model	$C_{H\alpha}$, $\sigma_{H\alpha}$						
	$Z = 0.0001$	$Z = 0.0003$	$Z = 0.001$	$Z = 0.004$	$Z = 0.01$	$Z = 0.02$	$Z = 0.03$
A	-41.462, 0.007	-41.419, 0.007	-41.361, 0.008	-41.266, 0.008	-41.163, 0.008	-41.056, 0.010	-41.008, 0.009
B	-41.366, 0.007	-41.311, 0.007	-41.247, 0.008	-41.129, 0.010	-41.022, 0.011	-40.894, 0.014	-40.849, 0.014
	$Z = 0.0001$	0.0004	0.004	0.008	0.02	0.05	0.1
C-S55	-41.387, 0.006	-41.282, 0.007	-41.218, 0.007	-41.174, 0.007	-41.078, 0.006	-40.938, 0.011	
C-Cha03	-41.608, 0.005	-41.503, 0.006	-41.442, 0.006	-41.398, 0.006	-41.303, 0.005	-41.159, 0.010	
D-S55		-41.236, 0.000	-41.134, 0.000	-41.066, 0.000	-40.922, 0.000	-40.693, 0.000	
D-K93'		-41.434, 0.000	-41.334, 0.000	-41.267, 0.000	-41.122, 0.000	-40.891, 0.000	
E-S55	-41.384, 0.001	-41.305, 0.001	-41.224, 0.001	-41.160, 0.001	-41.087, 0.001	-40.938, 0.001	-40.950, 0.001
E-K93'	-41.085, 0.001	-40.997, 0.001	-40.899, 0.001	-40.834, 0.001	-40.758, 0.001	-40.617, 0.001	-40.649, 0.001
F-S55'	-41.414, 0.285	-41.394, 0.298	-41.197, 0.213	-41.136, 0.170	-41.035, 0.133	-40.920, 0.090	
F-K01	-41.595, 0.398	-41.538, 0.399	-41.332, 0.309	-41.231, 0.264	-41.092, 0.189	-40.986, 0.150	

on the $SFR(L_{H\alpha})$ calibration. From Fig. 1, we see that the calibration curve of Model A locates below that of Model B at all Z , and the distance from the calibration curve of Model A to Model B increases with Z . Why the calibration curve of Model A locates below that of Model B and the effect of binary interactions increases with Z ? The reason is that binary interactions can produce some hotter stars at all Z , the produced hotter stars have relatively significant contribution to the UV flux and $L_{H\alpha}$ at high Z because that the temperature of stars in SPs would decrease with increasing Z .

To quantitatively analyze the effects of binary interactions and metallicity on the conversion coefficient between SFR and $L_{H\alpha}$, we give a fitting relation between $\log(SFR)$ and $\log(L_{H\alpha})$ when $\log(SFR) \geq -11$ and $\Delta\log(SFR) \geq 0.05$ for Models A and B by the following form:

$$\log \frac{SFR_{H\alpha}}{(M_{\odot} \text{ yr}^{-1})} = \log \frac{L_{H\alpha}}{(\text{erg s}^{-1})} + C_{H\alpha}, \quad (6)$$

where $SFR_{H\alpha}$ means that it is calculated from $L_{H\alpha}$. This

form of fitting (equation 6) is the same as that of K98 and MPD98. In Table 2, we present the fitting coefficient ($C_{H\alpha}$) and the rms ($\sigma_{H\alpha}$) for all models, the results of Models A and B are presented in the second and the third lines.

From Table 2, we see that $C_{H\alpha}$ increases and $\sigma_{H\alpha}$ shows little change when increasing Z for both Models A and B. The inclusion of binary interactions makes $C_{H\alpha}$ smaller and the effect of binary interaction increases with Z , this also can be seen from the first line of Table 3, in which we give the differences in the conversion coefficients between Models A and B, $\Delta C_{\text{case, BI}}$, at different metallicities. The inclusion of binary interactions makes $C_{H\alpha}$ smaller by ~ 0.1 dex at $Z=10^{-3}$ and ~ 0.2 dex at $Z=0.03$.

Comparing the conversion coefficient at different metallicities for a given set of models, we can obtain the effect of metallicity on the SFR calibration. In the second column of Table 4, we give the differences in the conversion coefficients $\Delta C_{\text{case, Z}}$ between at the highest and lowest metallicities ($\Delta[Fe/H]$) and $\Delta C_{\text{case, Z}}/\Delta[Fe/H]$ for all models. From

Table 3. Differences in the conversion coefficients between Models A and B, $\Delta C_{\text{case, BI}}$, in terms of $L_{\text{H}\alpha}$, L_{1500} , L_{2800} , $L_{[\text{OII}]}$ and L_{FIR} at metallicity $Z=0.0001, 0.0003, 0.001, 0.004, 0.01, 0.02$ and 0.03 (i.e. the effect of binary interactions).

$\Delta C_{\text{case, BI}}(\text{dex})$	$Z=0.0001$	0.0003	0.001	0.004	0.01	0.02	0.03
$\Delta C_{\text{H}\alpha, \text{BI}}$	0.096	0.108	0.114	0.138	0.141	0.161	0.160
$\Delta C_{1500, \text{BI}}$	0.077	0.071	0.069	0.063	0.063	0.069	0.067
$\Delta C_{2800, \text{BI}}$	0.156	0.134	0.113	0.087	0.074	0.072	0.070
$\Delta C_{[\text{OII}], \text{BI}}$	0.096	0.108	0.114	0.138	0.141	0.161	0.160
$\Delta C_{\text{FIR}, \text{BI}}$	~ 0.050	~ 0.050	~ 0.050	~ 0.050	~ 0.050	~ 0.050	~ 0.050

Table 4. Differences in the conversion coefficients between at the lowest and highest metallicities $\Delta C_{\text{case, Z}}$, $\Delta C_{\text{case, Z}}/\Delta[\text{Fe}/\text{H}]$ (the second column) and the variation rates of the conversion coefficients with metallicity $dC_{\text{case, Z}}/d[\text{Fe}/\text{H}]$ (from the third to the last columns) for Models A, B, C-S55/Cha03, D-S55/K93', E-S55/K93' and F-S55'/K01 (only for the case of $L_{\text{H}\alpha}$). The top, middle and bottom parts are for the cases of $C_{\text{H}\alpha}$, C_{1500} and C_{2800} , respectively. In each part, the top and bottom sub-parts are for Models A-B and C-F/E, respectively. Moreover, in each sub-part, the metallicity ranges are given in the first line.

Model	$\Delta C_{\text{H}\alpha, \text{Z}}, \frac{\Delta C_{\text{H}\alpha, \text{Z}}}{\Delta[\text{Fe}/\text{H}]}$ (dex)						
		[Fe/H]:-2.3~-1.8	-1.8~-1.3	-1.3~-0.7	-0.7~-0.3	-0.3~ 0.0	0.0~0.2
A	0.4537, 0.181	0.0870	0.1158	0.1573	0.2577	0.3590	0.2355
B	0.5171, 0.207	0.1106	0.1282	0.1963	0.2675	0.4253	0.2265
		[Fe/H]:-2.3~-1.7	-1.7~-0.7	-0.7~-0.4	-0.4~ 0.0	0.0~ 0.4	0.4~ 0.7
C-S55	0.4486, 0.166	0.1743	0.0646	0.1467	0.2378	0.3507	...
C-Cha03	0.4488, 0.166	0.1742	0.0615	0.1440	0.2400	0.3590	...
D-S55	0.5434, 0.259	...	0.1019	0.2253	0.3600	0.5748	...
D-K93'	0.5426, 0.258	...	0.0994	0.2240	0.3638	0.5762	...
E-S55	0.4344, 0.145	0.1313	0.0811	0.2120	0.1845	0.3722	-0.0393
E-K93'	0.4358, 0.145	0.1463	0.0976	0.2173	0.1900	0.3515	-0.1047
F-S55'	0.4939, 0.183	0.0332	0.1974	0.2037	0.2513	0.2875	...
F-K01	0.6092, 0.226	0.0962	0.2060	0.3353	0.3470	0.2653	...
Model	$\Delta C_{1500, \text{Z}}, \frac{\Delta C_{1500, \text{Z}}}{\Delta[\text{Fe}/\text{H}]}$ (dex)						
		[Fe/H]:-2.3~-1.8	-1.8~-1.3	-1.3~-0.7	-0.7~-0.3	-0.3~ 0.0	0.0~0.2
A	0.2787, 0.111	0.0598	0.0686	0.1177	0.1388	0.1887	0.1590
B	0.2691, 0.108	0.0478	0.0648	0.1077	0.1390	0.2067	0.1530
		[Fe/H]:-2.3~-1.7	-1.7~-0.7	-0.7~-0.4	-0.4~ 0.0	0.0~ 0.4	0.4~ 0.7
C-S55	0.2140, 0.080	0.0593	0.0535	0.0627	0.1393	0.1260	...
C-Cha03	0.2011, 0.074	0.0547	0.0502	0.0537	0.1342	0.1207	...
D-S55	0.1992, 0.095	...	0.0525	0.1137	0.1260	0.1555	...
D-K93'	0.1895, 0.090	...	0.0485	0.1073	0.1178	0.1543	...
E-S55	0.2401, 0.080	0.0258	0.0421	0.0913	0.1120	0.1745	0.1350
E-K93'	0.3232, 0.108	0.0520	0.0678	0.1513	0.1650	0.2003	0.1090
Model	$\Delta C_{2800, \text{Z}}, \frac{\Delta C_{2800, \text{Z}}}{\Delta[\text{Fe}/\text{H}]}$ (dex)						
		[Fe/H]:-2.3~-1.8	-1.8~-1.3	-1.3~-0.7	-0.7~-0.3	-0.3~ 0.0	0.0~0.2
A	0.3372, 0.135	0.0688	0.1258	0.1590	0.1665	0.1853	0.1115
B	0.2515, 0.101	0.0264	0.0830	0.1152	0.1337	0.1807	0.1000
		[Fe/H]:-2.3~-1.7	-1.7~-0.7	-0.7~-0.4	-0.4~ 0.0	0.0~ 0.4	0.4~ 0.7
C-S55	0.1647, 0.061	0.0487	0.0614	0.0437	0.0850	0.0675	...
C-Cha03	0.1474, 0.055	0.0432	0.0564	0.0333	0.0773	0.0605	...
D-S55	0.1381, 0.066	...	0.0490	0.0960	0.0760	0.0747	...
D-K93'	0.1250, 0.060	...	0.0444	0.0883	0.0645	0.0707	...
E-S55	0.2034, 0.068	0.0342	0.0455	0.0777	0.0802	0.1108	0.1257
E-K93'	0.3041, 0.101	0.0593	0.0764	0.1457	0.1468	0.1485	0.1010

Table 5. Similar to Table 2, but for C_{1500} and for Models A, B, C-S55/Cha03, D-S55/K93' and E-S55/K93'. The top and bottom parts are for Models A-B and C-E, respectively.

Model	C_{1500}, σ_{1500}						
	$Z=0.0001$	$Z=0.0003$	$Z=0.001$	$Z=0.004$	$Z=0.01$	$Z=0.02$	$Z=0.03$
A	-28.315, 0.086	-28.285, 0.072	-28.251, 0.061	-28.180, 0.032	-28.125, 0.024	-28.068, 0.022	-28.036, 0.016
B	-28.238, 0.048	-28.214, 0.044	-28.182, 0.039	-28.117, 0.025	-28.062, 0.017	-28.000, 0.011	-27.969, 0.009
	$Z=0.0001$	0.0004	0.004	0.008	0.02	0.05	0.1
C-S55	-28.120, 0.045	-28.084, 0.039	-28.031, 0.027	-28.012, 0.023	-27.956, 0.019	-27.906, 0.017	
C-Cha03	-28.309, 0.042	-28.276, 0.037	-28.226, 0.026	-28.210, 0.022	-28.156, 0.019	-28.108, 0.017	
D-S55		-28.033, 0.029	-27.980, 0.016	-27.946, 0.011	-27.896, 0.007	-27.834, 0.005	
D-K93'		-28.198, 0.027	-28.150, 0.015	-28.118, 0.011	-28.070, 0.006	-28.009, 0.005	
E-S55	-28.099, 0.032	-28.084, 0.026	-28.042, 0.015	-28.014, 0.010	-27.969, 0.006	-27.900, 0.003	-27.859, 0.002
E-K93'	-28.038, 0.054	-28.007, 0.045	-27.939, 0.026	-27.894, 0.018	-27.828, 0.010	-27.747, 0.005	-27.715, 0.003

Table 6. Similar to Table 2, but for C_{2800} and for Models A, B, C-S55/Cha03, D-S55/K93' and E-S55/K93'. The top and bottom parts are for Models A-B and C-E, respectively.

Model	C_{2800}, σ_{2800}						
	$Z=0.0001$	$Z=0.0003$	$Z=0.001$	$Z=0.004$	$Z=0.01$	$Z=0.02$	$Z=0.03$
A	-28.337, 0.268	-28.303, 0.232	-28.240, 0.185	-28.145, 0.120	-28.078, 0.087	-28.022, 0.068	-28.000, 0.053
B	-28.182, 0.097	-28.169, 0.086	-28.127, 0.070	-28.058, 0.049	-28.004, 0.034	-27.950, 0.023	-27.930, 0.018
	$Z=0.0001$	0.0004	0.004	0.008	0.02	0.05	0.1
C-S55	-28.003, 0.093	-27.974, 0.078	-27.912, 0.047	-27.899, 0.036	-27.865, 0.027	-27.838, 0.020	
C-Cha03	-28.183, 0.087	-28.157, 0.073	-28.101, 0.044	-28.091, 0.034	-28.060, 0.026	-28.036, 0.020	
D-S55		-27.920, 0.063	-27.871, 0.037	-27.842, 0.027	-27.812, 0.015	-27.782, 0.010	
D-K93'		-28.078, 0.059	-28.033, 0.035	-28.007, 0.025	-27.981, 0.014	-27.953, 0.009	
E-S55	-28.001, 0.072	-27.981, 0.058	-27.935, 0.033	-27.912, 0.023	-27.880, 0.013	-27.836, 0.006	-27.798, 0.004
E-K93'	-27.986, 0.113	-27.950, 0.093	-27.874, 0.055	-27.830, 0.039	-27.771, 0.022	-27.712, 0.011	-27.682, 0.008

the second and the third lines of the top part, we can that the discrepancy in $C_{H\alpha}$ between at $Z=0.0001$ and 0.03 can reach ~ 0.45 dex and ~ 0.52 dex, $\Delta C_{H\alpha, Z}/\Delta[\text{Fe}/\text{H}]$ are ~ 0.18 and ~ 0.21 for Models A and B, respectively, i.e. the inclusion of binary interactions lowers the sensitivity of metallicity to $C_{H\alpha}$. However, the variation rate of conversion coefficient with metallicity ($dC_{\text{case}, Z}/d[\text{Fe}/\text{H}]$) is different within different metallicity ranges, thus we give them in the 3rd-8th columns of Table 4. From the second and the third lines of the top part, we see that $dC_{H\alpha, Z}/d[\text{Fe}/\text{H}]$ reaches the maximal value near the solar metallicity (~ 0.36 and ~ 0.43).

3.2 SFR versus L_{1500} and SFR versus L_{2800}

In Fig. 2, we give the relations between $\log(\text{SFR})$ and the logarithmic UV luminosities at 1500 and 2800 Å of E, S0-Sd types of galaxies for Models A and B. For the sake of clarity, only the results at $Z=0.0001$ and 0.03 are presented in Fig. 2. Also shown are the results of K98, Madau et al. (1998, hereafter MPD98) and Gilbank et al. (2010, hereafter G10). K98 gives $\text{SFR}_{\text{UV}}/\text{M}_{\odot}\text{yr}^{-1} = 1.4 \times 10^{-28} L_{i, \text{UV}}/\text{erg s}^{-1} \text{Hz}^{-1}$, MPD98 gives $\text{SFR}_{\text{UV}}/\text{M}_{\odot}\text{yr}^{-1} = C \times 10^{-28} L_{i, \text{UV}}/\text{erg s}^{-1} \text{Hz}^{-1}$, where $C=(1.25, 2.86)$ for L_{1500} and $C=(1.26, 1.96)$ for L_{2800} when using the IMFs of S55 and Scalo (1986), and G10 gives $\text{SFR}_{\text{UV}}/\text{M}_{\odot}\text{yr}^{-1} = 0.71 \times 10^{-28} L_{i, \text{UV}}/\text{erg s}^{-1} \text{Hz}^{-1}$.

First, from the left-hand panel of Fig. 2, we see that at $Z=0.03$, L_{1500} varies linearly with SFR (in comparison

with the lines of K98, MPG98 and G10) and the SFR(L_{1500}) calibration curves overlap (coincide) for all galaxy types (from E to Sd) for both Models A and B. The inclusion of binary interactions can lower the conversion coefficient by the same amount for all galaxy types. At $Z=0.0001$, the calibration curves do not display the same calibration relation for all galaxy types (out of alignment/not in a line, the difference of ~ 0.4 dex), only display a linear relation for the late types. The earlier (i.e. τ decreases) is the galaxy type, the more is the deviation from the linear SFR- L_{1500} relation (the larger is the slope of calibration curve) and the lower is the location of the SFR(L_{1500}) calibration curve.

From the right-hand panel of Fig. 2, we see that the SFR(L_{2800}) calibration is similar to that of SFR(L_{1500}), but there are two exceptions. One is at $Z=0.03$, the SFR(L_{2800}) calibration is not unique for all galaxy types (the difference of less than 0.05 dex), while is unique for the SFR(L_{1500}) calibration. The second is at $Z=0.0001$, the calibration curves do not display a linear calibration relation for all galaxy types, while only for the early types in the case of L_{1500} . Moreover, the deviation from the linear SFR- L_{2800} relation (slope > 1) is far larger than that in the case of L_{1500} . This phenomenon means that L_{2800} can not be used in the linear calibration of SFR at low-metallicity end.

Also, for the purpose of quantitative analyse, in Tables 5 and 6, we give the linear fitting coefficients (C_{1500} and C_{2800}) and rms (σ_{1500} and σ_{2800}) between $\log(\text{SFR})$ and $\log(L_{1500})$ and between $\log(\text{SFR})$ and $\log(L_{2800})$ for all mod-

els. From the second and the third lines of Tables 5 and 6, we see that C_{1500} and C_{2800} increase and σ_{1500} and σ_{2800} decrease when increasing Z for both Models A and B. The relative large rms at low metallicities is caused by the non-unique relation among all galaxy types and the non-linear relation between $\log(\text{SFR})$ and $\log(L_{i,\text{UV}})$ for both Models A and B.

From the differences in the C_{1500} and C_{2800} between Models A and B ($\Delta C_{1500,\text{BI}}$ and $\Delta C_{2800,\text{BI}}$) at different metallicities, which are presented in the second and the third lines of Table 3, we see that the effect of binary interactions does not vary with Z for C_{1500} (~ 0.07 dex) and decreases with Z for C_{2800} ($0.16 \rightarrow 0.07$ dex).

At last, from the second and the third lines in the middle and bottom parts of Table 4, we see that the discrepancy in C_{1500} between at $Z=0.0001$ and 0.03 reaches ~ 0.28 dex and ~ 0.27 dex, that in C_{2800} reaches ~ 0.34 dex and ~ 0.25 dex, $\Delta C_{1500,Z}/\Delta[\text{Fe}/\text{H}]$ is ~ 0.11 and ~ 0.11 and $\Delta C_{2800,Z}/\Delta[\text{Fe}/\text{H}]$ is ~ 0.14 and ~ 0.10 for Models A and B, respectively, i.e. the inclusion of binary interactions raises the sensitivity of metallicity to the $\text{SFR}(L_{2800})$ calibration. The $dC_{1500,Z}/d[\text{Fe}/\text{H}]$ and $dC_{2800,Z}/d[\text{Fe}/\text{H}]$ are different within different metallicity ranges and also reach the maximal value near the solar metallicity (~ 0.20) for Models A and B.

3.3 SFR versus $L_{[\text{OII}]}$

In this work, the luminosity of the $[\text{OII}]\lambda 3727\text{\AA}$ forbidden line doublet, $L_{[\text{OII}]}$, is obtained by using the empirical ratio $L_{[\text{OII}]} / L_{\text{H}\alpha} = 0.23$, which is used in the work of Hopkins et al. (2003). Because the fixed $L_{[\text{OII}]} / L_{\text{H}\alpha}$ ratio is used, the $\text{SFR}(L_{[\text{OII}]})$ calibration curve moves upwards by an amount of $\lg(1/0.23)$ in comparison with that of $\text{SFR}(L_{\text{H}\alpha})$ in Fig. 1. The effects of binary interactions and metallicity on the $\text{SFR}(L_{[\text{OII}]})$ calibration are the same as those on the $\text{SFR}(L_{\text{H}\alpha})$ calibration. In the fourth line of Table 3, we give the difference in $C_{[\text{OII}]}$ between Models A and B at different metallicities.

3.4 SFR versus L_{FIR}

For the SFR calibrations in terms of L_{FIR} , it is from the models with constant SFR under the assumption of the bolometric luminosity $L_{\text{BOL}} = L_{\text{FIR}}$.

In Fig. 3, we give the L_{FIR} evolution of Irr galaxies (i.e. models with constant SFR) for Models A and B. For the sake of clarity, only the results at $Z=0.0001, 0.001, 0.01$ and 0.03 are presented. Also shown are the result of K98 ($\text{SFR}_{\text{FIR}}/\text{M}_{\odot}\text{yr}^{-1} = 4.5 \times 10^{-44} L_{\text{FIR}}/\text{erg s}^{-1}$). From it, we see that SFR does not vary linearly with L_{FIR} , the inclusion of binary interactions raises the L_{FIR} by about 0.05 dex at all metallicities (see the fifth line of Table 3). The lower is the metallicity, the larger is the deviation from the linear $\text{SFR}-L_{\text{FIR}}$ relation. The effect of metallicity on the $\text{SFR}(L_{\text{FIR}})$ calibration reaches ~ 0.3 dex.

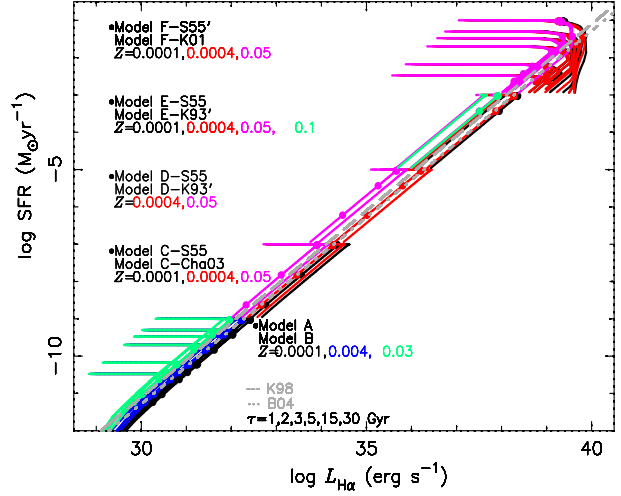


Figure 4. Relation between SFR and $L_{\text{H}\alpha}$ for Models A (solid circles), B, C-S55 (circles), C-Cha03, D-S55 (circles), D-K93', E-S55 (circles), E-K93', F-S55' (circles) and F-K01 at different metallicities. For Models C-F, the results are moved upwards along the diagonal line, respectively. For Models A/B and F-S55'/K01, E, S0 and Sa-Sd types (from top to bottom) are included, while for Models C-S55/Cha03, D-S55/K93' and E-S55/K93', only E type is included. For Models A/B, $Z=0.0001$ (black), 0.004 (blue) and 0.03 (green, from right to left) are included, for Models C-S55/Cha03 and F-S55'/K01, $Z=0.0001$ (black), 0.0004 (red) and 0.05 (magenta) are included, for Models D-S55/K93', $Z=0.0004$ (red) and 0.05 (magenta) are included, and for Models E-S55/K93', $Z=0.0001$ (black), 0.0004 (red), 0.05 (magenta) and 0.1 (green) are included. Note the color is the same at a given Z . At last, also shown are the results of K98 (grey dashed line) and B04 (grey dotted line).

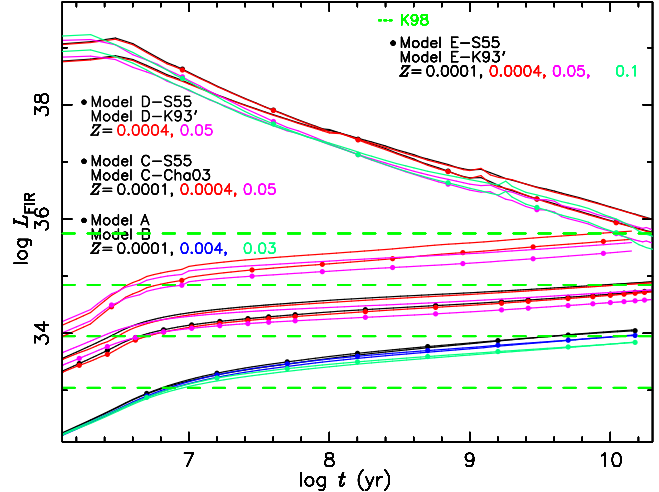


Figure 6. The L_{FIR} evolution of Irr galaxies (i.e. models with constant star formation, $\text{SFR}=1 \text{ M}_{\odot}$) for Models A/B, C-S55/C-Cha03, D-S55/D-K93' and E-S55/E-K93'. The line colour and symbol have the same meanings as in Fig. 4. Also shown is the result of K98 (green dashed line). The results of Models C-E and K98 are moved upwards, respectively.

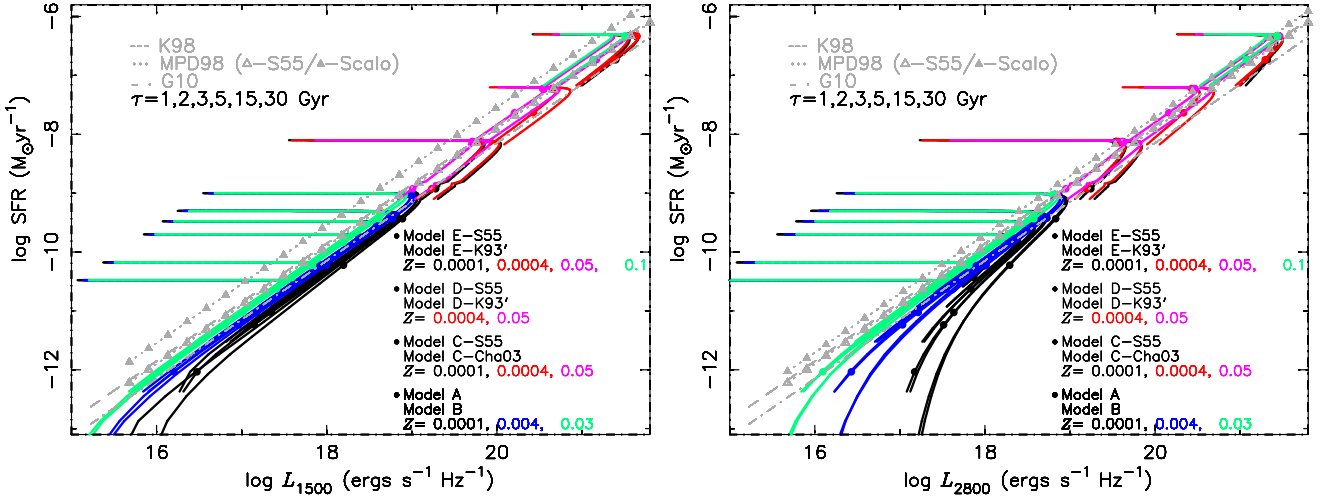


Figure 5. Relations between SFR and $L_{i,UV}$ for Models A/B, C-S55/C-Cha03, D-S55/D-K93' and E-S55/E-K93' at different metallicities. Left-hand panel is for L_{1500} and right-hand panel is for L_{2800} . The line colour and symbol have the same meanings as in Fig. 4. For Models C-E, the results are moved upwards along the diagonal line, respectively. Also shown are the results of K98 (grey dashed line), MPD98 (grey dotted line, open and solid triangles are for using the S55 and Scalo IMFs, respectively) and G10 (grey dash-dotted line).

Table 7. Differences in the conversion coefficients between by using the two IMFs, $\Delta C_{case,IMF}$, for Models C, D, E and F (only for $C_{H\alpha}$) at metallicity $Z=0.0001, 0.0004, 0.004, 0.008, 0.02, 0.05$ and 0.1 . The top, middle and bottom parts are for the cases of $\Delta C_{H\alpha}$, ΔC_{1500} and ΔC_{2800} , respectively.

Model	0.0001	0.0004	0.004	0.008	0.02	0.05	0.1
$\Delta C_{H\alpha,IMF}$ (dex)							
C	-0.221	-0.221	-0.224	-0.225	-0.224	-0.221	
D		-0.198	-0.200	-0.201	-0.199	-0.199	
E	0.299	0.308	0.325	0.326	0.329	0.320	0.301
F	-0.181	-0.143	-0.135	-0.095	-0.057	-0.066	
$\Delta C_{1500,IMF}$ (dex)							
C	-0.190	-0.192	-0.196	-0.198	-0.200	-0.202	
D		-0.165	-0.169	-0.171	-0.174	-0.175	
E	0.061	0.077	0.103	0.121	0.142	0.152	0.144
$\Delta C_{2800,IMF}$ (dex)							
C	-0.180	-0.184	-0.189	-0.192	-0.195	-0.198	
D		-0.158	-0.162	-0.165	-0.169	-0.171	
E	0.015	0.030	0.061	0.082	0.108	0.123	0.116

Table 8. The differences in the conversion coefficients, $\Delta C_{case,factor}$, caused by the adoption of different EPS models, metallicity and IMF.

Case	EPS	Z	IMF
$\Delta C_{H\alpha,factor}$ (dex)	~ 0.2	0.43-0.61	0.06-0.33
$\Delta C_{1500,factor}$ (dex)	~ 0.2	0.19-0.32	0.06-0.20
$\Delta C_{2800,factor}$ (dex)	~ 0.2	0.13-0.34	0.02-0.20
$\Delta C_{FIR,factor}$ (dex)	~ 1.2	$\sim 0.3-0.6$	small

4 SFR CALIBRATIONS BY USING THE OTHER EPS MODELS

To discuss the effect of metallicity on the SFR calibrations when using the other EPS models and compare them with our results, in this section we will present the $SFR(L_{H\alpha})$, $SFR(L_{i,UV})$, $SFR(L_{[OII]})$ and $SFR(L_{FIR})$ calibrations by using the BC03, *SB99*, *PÉGASE* and POPSTAR EPS models. These EPS models (including the used parameters, physics, IMF, M_1 , M_u and metallicity) have been described in Section 2. These four sets of results are referred to as Models C,

D, E and F, respectively. For each set of results, two subsets are considered, depending on the IMF. To distinguish them, the name of used IMF is the supplement to the model name (see the first column of Table 1).

In this section, we first obtain the $L_{H\alpha}$, $L_{i,UV}$, $L_{[OII]}$ and L_{FIR} of burst, E, S0, Sa-Sd and Irr types of galaxies by using the above EPS models at their own metallicities (see the fifth column of Table 1), then give the linear fitting coefficients between $\log(SFR)$ and $\log(L_{H\alpha})$, between $\log(SFR)$ and $\log(L_{1500})$ and between $\log(SFR)$ and $\log(L_{2800})$ in Tables 2, 5 and 6, and their variation rates with metallicity in the upper, middle and bottom parts of Table 4.

4.1 SFR versus $L_{H\alpha}$

First, we study the relation between SFR and $L_{H\alpha}$ for Models C-S55/Cha01, D-S55/K93', E-S55/K93' and F-S55'/K01, and find that SFR varies linearly with $L_{H\alpha}$ (the slope $d(\log SFR)/d(\log L_{H\alpha}) \sim 1$) for all galaxy types, metallicities and models except the F-S55'/K01 models (SFR varies linearly with $L_{H\alpha}$ only for all types of metal-rich galaxies, while not true for E-Sd types of metal-poor galaxies). Therefore, for the sake of clarity, in Fig. 4 we only give the relation between $\log(SFR)$ and $\log(L_{H\alpha})$ of E, S0, Sa, Sb, Sc and Sd types for Models A/B at $Z=0.0001, 0.004$ and 0.03 and for Models F-S55'/K01' at $Z=0.0001, 0.0004$ and 0.05 , that of only E type for Models C-S55/Cha03 at $Z=0.0001, 0.0004$ and 0.05 , for Models D-S55/K93' at $Z=0.0004$ and 0.05 and for Models E-S55/K93' at $Z=0.0001, 0.0004, 0.05$ and 0.1 . The reason we choose these metallicities (highlighted in red in Table 1) for a given set of models is that the value is either the upper/lower limit or the common one. Moreover, for the sake of clarity, the $\log(SFR)$ versus $\log(L_{H\alpha})$ calibration curves of Models C-F in Fig. 4 are moved upwards along the diagonal line [i.e. $\log(SFR)$ and $\log(L_{H\alpha})$ are multiplied by the same factor for a given set of models]. At last, we also give the results of K98 and B04 in Fig. 4.

From Fig. 4, we see exactly that the slope

$\text{dlog(SFR)}/\text{dlog}(L_{\text{H}\alpha})$ is similar to those of K98 and B04 for all models at all Z (except Models F-S55'/K01 at low metallicities), i.e. SFR varies linearly with $L_{\text{H}\alpha}$ at all Z . The slope of calibration curve for Models F-S55'/K01 deviates from those of K98 and B04 at low metallicities, i.e. $L_{\text{H}\alpha}$ does not vary linearly with SFR at low metallicities. The calibration curve moves upwards with increasing metallicity, i.e. the conversion factor increases (this also can be seen from the values in Table 2), but there are an exception: Models E-S55/K93' in the $[\text{Fe}/\text{H}]$ range from 0.4 to 0.7. The value of $\text{d}C_{\text{H}\alpha, Z}/\text{d}[\text{Fe}/\text{H}]$ is negative within this range for Model E (see the top panel of Table 4). The reason that $C_{\text{H}\alpha}$ increases with Z is that the temperature of stars decreases with increasing Z .

[Fe/H]: From the top part of Table 4, we see that the difference in the $C_{\text{H}\alpha}$ caused by metallicity, $\Delta C_{\text{H}\alpha, Z}$, reaches $\sim 0.43\sim 0.61$ dex, $\Delta C_{\text{H}\alpha, Z}/\Delta[\text{Fe}/\text{H}]$ is within $\sim 0.15\sim 0.26$, $\text{d}C_{\text{H}\alpha, Z}/\text{d}[\text{Fe}/\text{H}]$ is different within different $[\text{Fe}/\text{H}]$ ranges and reaches the maximum value at high metallicity for all models. For Model D, $\Delta C_{\text{H}\alpha, Z}/\Delta[\text{Fe}/\text{H}]$ and the maximum value of $\text{d}C_{\text{H}\alpha, Z}/\text{d}[\text{Fe}/\text{H}]$ are the largest ($\text{d}C_{\text{H}\alpha, Z}/\text{d}[\text{Fe}/\text{H}]\sim 0.57$ in the $[\text{Fe}/\text{H}]$ range from 0.0 to 0.4) in comparison with the other models.

IMF: In Table 7, we give the differences in the conversion coefficients between by using the two IMFs, $\Delta C_{\text{case}, \text{IMF}}$, for Models C-F/E. From the top part, we see that $\Delta C_{\text{H}\alpha, \text{IMF}}$ is independent of Z for Models C, D and E ($=C_{\text{case}, \text{S55}/\text{S55}' - C_{\text{case}, \text{Cha03}/\text{K93}'}/\text{K01}$, ~ -0.2 , ~ -0.2 and ~ 0.3 dex, respectively), the absolute value for Model F decreases with increasing Z (~ 0.18 dex and ~ 0.07 dex at $Z=0.0001$ and 0.05 , respectively). The larger $\Delta C_{\text{H}\alpha, \text{IMF}}$ at low metallicities for Model F is caused by the deviation from the linear SFR- $L_{\text{H}\alpha}$ relation.

EPS and other: From Table 2, we see that the difference in the $C_{\text{H}\alpha}$ reaches ~ 0.55 dex at $Z=0.02$ among Models A-F [the 7th and the 6th column for Models A-B and C-F] and ~ 0.52 dex at $Z=0.0001$ among Models A-C and E [the second column, excluding Model F because of the non-linear SFR- $L_{\text{H}\alpha}$ relation]. This kind of difference is comparable to that caused by metallicity, and mainly is caused by the differences in the adoption of EPS models, the algorithm of obtaining $L_{\text{H}\alpha}$ and IMF.

From Table 2, we also see that the difference in the $C_{\text{H}\alpha}$ is ~ 0.18 dex among Models B, C-S55, D-S55, E-S55 and F-S55' at $Z=0.02$ and ~ 0.02 dex among Models B, C-S55 and E-S55 at $Z=0.0001$. That is to say, the difference in the $C_{\text{H}\alpha}$, caused by the adoptions of different EPS models and the algorithm of obtaining $L_{\text{H}\alpha}$, is less than 0.2 dex. For Models A-C and D, the algorithm of obtaining $L_{\text{H}\alpha}$ and the companied coefficients (see equation 11 in Paper I) are the same, so the difference in the corresponding EPS models produces the difference in $C_{\text{H}\alpha}$ among these models. For Model E, the algorithm of obtaining $L_{\text{H}\alpha}$ is different from that of Models A-D. For Model F, the algorithm is the same but the coefficients depend on Z and the electronic temperature. Therefore, it is the differences in the algorithm (including the coefficients) and EPS models that produce the difference in $C_{\text{H}\alpha}$.

4.2 SFR versus L_{1500} and SFR versus L_{2800}

In Fig. 5, we give the relations between $\log(\text{SFR})$ and $\log(L_{i, \text{UV}})$ for Models A, B, C-S55/Cha01, D-S55/K93' and E-S55/K93'. For a given set of models, the selected galaxy types and metallicities are the same as those in Fig. 4. Similarly, the results of Models C, D and E are moved upwards along the diagonal line. In Fig. 5, we also give the results of K98, MPD98 and G10.

From the left- and right-hand panels of Fig. 5, we see that the calibration curves of SFR versus L_{1500} and SFR versus L_{2800} for Models C, D and E are similar to the corresponding ones for Models A and B. SFR varies linearly with L_{1500} and L_{2800} [the slope $\log(\text{SFR})/\log(L_{i, \text{UV}}) \sim 1$, in comparison with those of K98, MPD98 and G10] at all metallicities except the early types at low metallicities (more significant for L_{2800}), and at $Z=0.0001$ the SFR($L_{i, \text{UV}}$) calibration is not unique for all galaxy types. The conversion coefficients increase with increasing Z . The linear fitting coefficients, between SFR and L_{1500} and between SFR and L_{2800} , are presented in Tables 5 and 6, respectively.

[Fe/H]: From the middle part of Table 4, we see that the $\Delta C_{1500, Z}$ and $\Delta C_{1500, Z}/\Delta[\text{Fe}/\text{H}]$ are in the ranges of $\sim 0.19\sim 0.32$ dex and $\sim 0.07\sim 0.11$ for all models. Both values are the largest for Model E-S55'. From the bottom part of Table 4, we see that $\Delta C_{2800, Z}$ and $\Delta C_{2800, Z}/\Delta[\text{Fe}/\text{H}]$ are within $\sim 0.13\sim 0.34$ dex and $\sim 0.06\sim 0.14$ for Models A-E. For a given set of models, the value of $\Delta C_{1500, Z}/\Delta[\text{Fe}/\text{H}]$ is greater than $\Delta C_{2800, Z}/\Delta[\text{Fe}/\text{H}]$, i.e. L_{1500} is more sensitive to metallicity. Also, $\text{d}C_{1500, Z}/\text{d}[\text{Fe}/\text{H}]$ and $\text{d}C_{2800, Z}/\text{d}[\text{Fe}/\text{H}]$ are different within different $[\text{Fe}/\text{H}]$ ranges and reach the maximum value near the solar metallicity (similar to that of $\text{d}C_{\text{H}\alpha}/\text{d}[\text{Fe}/\text{H}]$).

IMF: From the middle and bottom parts of Table 7, we see that $\Delta C_{1500, \text{IMF}}$ and $\Delta C_{2800, \text{IMF}}$ are independent of Z for Models C and D (~ -0.2 dex and ~ -0.17 dex, respectively). The absolute $\Delta C_{1500, \text{IMF}}$ and $\Delta C_{2800, \text{IMF}}$ decrease with increasing Z for Model E (difference of ~ 0.1 dex), this is different from the case of $\Delta C_{\text{H}\alpha, \text{IMF}}$ for Model E (independent of Z). Similarly, the larger $\Delta C_{1500, \text{IMF}}$ and $\Delta C_{2800, \text{IMF}}$ at low metallicities for Model E are partly caused by the non-unique relation for all galaxy types and non-linear relation between SFR and $L_{i, \text{UV}}$.

EPS: From the SFR(L_{1500}) and SFR(L_{2800}) calibration curves in Fig. 5 and the conversion coefficients in Tables 5 and 6 for all models, we see that the differences in C_{1500} and C_{2800} are ~ 0.33 and 0.29 dex at $Z=0.02$ for Models A-E [the 7th and 6th column for Models A-B and C-E] and ~ 0.28 and 0.33 dex at $Z=0.0001$ among Models A-C and E [the second column, comparable to those caused by metallicity]. Also the differences are mainly caused by the differences in the IMF and the adoption of EPS models. From Tables 5 and 6, we see that the differences in C_{1500} and C_{2800} are ~ 0.10 and 0.24 dex among Models B, C-S55 D-S55 and E-S55 at $Z=0.02$ and ~ 0.14 and 0.18 dex at $Z=0.0001$ among Models B, C-S55 and E-S55, so the adoption of EPS models causes to the difference of ~ 0.2 dex in the C_{1500} and C_{2800} .

4.3 SFR versus L_{FIR}

In Fig. 6, we give the evolution of bolometric magnitude of Irr galaxies for Models A, B, C, D and E. For a given set of

models, the selected galaxy types and metallicities are the same as those in Fig. 4. Also shown are the result of K98. Similarly, the results of Models C, D and E and the result of K98 are moved upwards.

From Fig. 6, we see that the effect of metallicity on the SFR versus L_{FIR} calibration for Models C-E is similar to that for Models A-B: C_{FIR} increases with increasing Z , the difference in the conversion factor by metallicity reaches ~ 0.3 - 0.6 dex. The difference in C_{FIR} caused by EPS models reaches ~ 1.2 dex, which is two/more times larger than that caused by metallicity. The difference in C_{FIR} caused by IMF is insignificant in comparison with that caused by EPS model and metallicity.

4.4 Comparison among various effects

In this part, we will summary and compare the effects of EPS models, metallicity and IMF on the conversion coefficients. From Section 4.1-4.3, we see that the differences in the $C_{\text{H}\alpha}$, C_{1500} , C_{2800} and C_{FIR} among Models A-E/F reach ~ 0.5 , ~ 0.3 , ~ 0.3 and ~ 1.2 dex. However, after excluding the effects of IMF and algorithm, we see that the differences in $C_{\text{H}\alpha}$, C_{1500} , C_{2800} and C_{FIR} , which solely caused by EPS models, are ~ 0.2 , ~ 0.2 , ~ 0.2 and ~ 1.2 dex.

In Table 8, we summary the differences in the conversion coefficients caused by the adoption of different EPS models, metallicity and IMF. The values in the 3rd-4th columns of Table 8 are from Tables 4 and 7, respectively. From it, we see that the difference in the $C_{\text{H}\alpha}$ caused by metallicity is two times larger than that caused by the adoption of different EPS models and IMF (the first line). The difference in the SFR(L_{FIR}) calibration caused by the adoption of EPS models is two/more times larger than that caused by metallicity, and the effect of IMF on the SFR(L_{FIR}) calibration is small (the last line). As for $\Delta C_{i,\text{UV}}$, the effects of EPS models, IMF and metallicity are comparable.

5 SUMMARY AND CONCLUSIONS

Using the Yunnan EPS models with and without binary interactions, we present the $L_{\text{H}\alpha}$, $L_{[\text{OII}]}$, $L_{i,\text{UV}}$ and L_{FIR} for burst, E, S0, Sa-Sd and Irr galaxies, the conversion coefficients between SFR and these diagnostics at $Z = 0.0001$, 0.0003 , 0.001 , 0.004 , 0.01 , 0.02 and 0.03 , and discuss the effects of binary interactions and metallicity on these calibrations of SFR. Our conclusions are as follows. (i) The $L_{i,\text{UV}}$ is not suitable to the linear calibration of SFR at low metallicities. (ii) The effect of binary interactions on the SFR calibrations is as follows. The inclusion of binary interactions lowers the SFR versus $L_{\text{H}\alpha}$ and SFR versus $L_{[\text{OII}]}$ conversion factors by ~ 0.1 - 0.2 dex, the SFR versus L_{1500} by ~ 0.1 dex, the SFR versus L_{2800} by ~ 0.2 - 0.1 dex, but raises the SFR versus L_{FIR} by ~ 0.05 dex. The differences in these conversion coefficients are dependent of metallicity for $L_{\text{H}\alpha}$, $L_{[\text{OII}]}$ and L_{2800} , independent for L_{1500} and L_{FIR} . The higher is the metallicity, the larger are the differences in the SFR versus $L_{\text{H}\alpha}$ and SFR versus $L_{[\text{OII}]}$ conversion factors, while the smaller is the difference in the SFR versus L_{2800} conversion coefficient. (iii) The effect of metallicity on the SFR calibrations is as follows. $\Delta C_{\text{case},Z}/\Delta[\text{Fe}/\text{H}]$ reaches ~ 0.2 for $L_{\text{H}\alpha}$ and $L_{[\text{OII}]}$, ~ 0.1 for $L_{i,\text{UV}}$ and ~ 0.1 - 0.2 for L_{FIR} .

The $dC_{\text{case},Z}/d[\text{Fe}/\text{H}]$ is different within different metallicity ranges and reaches the maximum value near the solar metallicity.

We also obtain the $L_{\text{H}\alpha}$, $L_{[\text{OII}]}$, $L_{i,\text{UV}}$ and L_{FIR} for burst, E, S0, Sa-Sd and Irr galaxies by using the BC03 ($0.0001 \leq Z \leq 0.05$), *SB99* ($0.0004 \leq Z \leq 0.05$), *PÉGASE* ($0.0001 \leq Z \leq 0.1$) and POPSTAR ($0.0001 \leq Z \leq 0.05$) models, and present the conversion coefficients between SFR and these diagnostics. For these models, we discuss the effects of IMF and metallicity on these SFR calibrations, and compare the conclusions with those from our models. By comparisons, we find that the conclusions are similar to ours. The relations between SFR and these diagnostics are linear at all metallicities (except $L_{\text{H}\alpha}$ when using the POPSTAR models), the conversion coefficients increase with Z (in the range of 0.13 - 0.61 dex, see the third column of Table 8) except $L_{\text{H}\alpha}$ when using the *PÉGASE* models within $[\text{Fe}/\text{H}] > 0$, and $dC_{\text{case},Z}/d[\text{Fe}/\text{H}]$ reaches the maximum value near the solar metallicity.

The differences in the SFR($L_{\text{H}\alpha}$), SFR($L_{i,\text{UV}}$) and SFR(L_{FIR}) calibrations caused by the adoption of different EPS models reach ~ 0.2 , 0.2 and 1.2 dex. The difference in the conversion coefficients caused by IMF, $\Delta C_{\text{case},\text{IMF}}$, is dependent of Z for $L_{\text{H}\alpha}$ when using the POPSTAR models and for $L_{i,\text{UV}}$ when using the *PÉGASE* models, but independent of Z for the other diagnostics and using the other EPS models (in the range of 0.02 - 0.33 dex, see the fourth column of Table 8). The differences in the SFR($L_{\text{H}\alpha}$) and SFR(L_{FIR}) calibrations are mainly caused by metallicity and EPS models, respectively. The effects of EPS models, metallicity and IMF on $\Delta C_{i,\text{UV}}$ are comparable.

ACKNOWLEDGEMENTS

This work was funded by the Chinese Natural Science Foundation (Grant Nos 11273053, 11073049, 11033008, 10821026 & 2007CB15406), by Yunnan Foundation (Grant No 2011CI053) and by the Chinese Academy of Sciences (KJXC2-YW-T24).

REFERENCES

- Aarseth S. J., 1999, *PASP*, 111, 1333
- Anders P., Baumgardt H., Gaburov E., Portegies Zwart S., 2012, *MNRAS*, 421, 3557
- Brinchmann J., Charlot S., White S. D. M., Tremonti C., Kauffmann G., Heckman T., Brinkmann J., 2004, *MNRAS*, 351, 1151
- Bruzual G., Charlot S., 2003, *MNRAS*, 344, 1000
- Chabrier G., 2003, *PASP*, 115, 763
- Crowther P., 2012, *Astronomy and Geophysics*, 53, 040000
- de Grijs R., Goodwin S. P., Kouwenhoven M. B. N., Kroupa P., 2008, *A&A*, 492, 685
- Eldridge J. J., 2012, *MNRAS*, 422, 794
- Fioc M., Rocca-Volmerange B., 1997, *A&A*, 326, 950
- Fioc M., Rocca-Volmerange B., 1999, *A&A*, 344, 393
- Gao Y., Solomon P. M., 2004, *ApJS*, 152, 63
- Gilbank D. G., Baldry I. K., Balogh M. L., Glazebrook K., Bower R. G., 2010, *MNRAS*, 405, 2594

- Hernández F. C., Bruzual G., 2011, in *Revista Mexicana de Astronomía y Astrofísica Conference Series*, Vol. 40, *Revista Mexicana de Astronomía y Astrofísica Conference Series*, pp. 277–277
- Hopkins A. M. et al., 2003, *ApJ*, 599, 971
- Hurley J. R., Pols O. R., Aarseth S. J., Tout C. A., 2005, *MNRAS*, 363, 293
- Kennicutt, Jr. R. C., 1998, *ARA&A*, 36, 189
- Kobulnicky H. A., Fryer C. L., 2007, *ApJ*, 670, 747
- Kouwenhoven M. B. N., Brown A. G. A., Portegies Zwart S. F., Kaper L., 2007, *A&A*, 474, 77
- Kroupa P., Aarseth S., Hurley J., 2001, *MNRAS*, 321, 699
- Kroupa P., Tout C. A., Gilmore G., 1993, *MNRAS*, 262, 545
- Leitherer C., Ortiz Otálvaro P. A., Bresolin F., Kudritzki R.-P., Lo Faro B., Pauldrach A. W. A., Pettini M., Rix S. A., 2010, *ApJS*, 189, 309
- Leitherer C. et al., 1999, *ApJS*, 123, 3
- Madau P., Pozzetti L., Dickinson M., 1998, *ApJ*, 498, 106
- Miller G. E., Scalo J. M., 1979, *ApJS*, 41, 513
- Mollá M., García-Vargas M. L., Bressan A., 2009, *MNRAS*, 398, 451
- Salpeter E. E., 1955, *ApJ*, 121, 161
- Sansom A. E., Izzard R. G., Ocvirk P., 2009, *MNRAS*, 399, 1012
- Scalo J. M., 1986, *Fundam. Cosmic Phys.*, 11, 1
- Spurzem R., 1999, *Journal of Computational and Applied Mathematics*, 109, 407
- Vázquez G. A., Leitherer C., 2005, *ApJ*, 621, 695
- Zhang F., Han Z., Li L., Hurley J. R., 2004, *A&A*, 415, 117
- Zhang F., Li L., Han Z., 2009, *MNRAS*, 396, 276
- Zhang F., Li L., Zhang Y., Kang X., Han Z., 2012, *MNRAS*, 421, 743

This paper has been typeset from a \LaTeX file prepared by the author.